American Society of Hematology
2021 L Street NW, Suite 900,
Washington, DC 20036
Phone: 202-776-0544 | Fax 202-776-0545
editorial@hematology.org

Functional mapping of PHF6 complexes in chromatin remodeling, replication dynamics and DNA repair.

Tracking no: BLD-2021-014103R1 - CORRECTION

Adolfo Ferrando (Columbia University, United States) Silvia Alvarez (Columbia University, United States) Ana da Silva Almeida (Biogen, United States) Robert Albero (Columbia University Medical Center, Spain) Angelica Barreto-Galvez (Rutgers Cancer Institute of New Jersey, United States) Thomas Gunning (Hackensack Meridian School of Medicine, United States) Mayukh Biswas (Columbia University, United States) Anam Shaikh (Rutgers Cancer Institute of New Jersey, United States) Tomas Aparicio (Columbia University, United States) Agnieszka Wendorff (Epic Bio, United States) Erich Piovan (University of Padua, Italy) Pieter Van Vlierberghe (Ghent University, Belgium) Steven Gygi (Harvard Medical School, United States) Jean Gautier (Columbia University Irving Medical Center, United States) Advaitha Madireddy (Rutgers Cancer Institute of New Jersey, United States)

Abstract:
The Plant Homeodomain 6 gene (*PHF6*) encodes a nucleolar and chromatin-associated leukemia tumor suppressor with proposed roles in transcription regulation. However, specific molecular mechanisms controlled by PHF6 remain rudimentarily understood. Here we show that PHF6 engages multiple nucleosome remodeling protein complexes including NuRD, SWI/SNF and ISWI factors, the replication machinery and DNA repair proteins. Moreover, following DNA damage, PHF6 localizes to sites of DNA injury and its loss impairs the resolution of DNA breaks with consequent accumulation of single- and double-stranded DNA lesions. Native chromatin immunoprecipitation sequencing analyses reveal that PHF6 specifically associates with difficult to replicate heterochromatin at satellite DNA regions enriched in Histone H3 lysine 9 trimethyl marks (H3K9me3) and single molecule locus-specific analyses identify PHF6 as an important regulator of genomic stability at fragile sites. These results extend our understanding of the molecular mechanisms controlling HSC homeostasis and leukemia transformation by placing PHF6 at the crossroads of chromatin remodeling, replicative fork dynamics and DNA repair.

Conflict of interest: No COI declared

COI notes:

Preprint server: No;

Author contributions and disclosures: SA and ADSA performed most of the experiments; RA and MB analyzed the ChIP-Seq data; SG analyzed mass-spectrometry data; TA performed immunostainings on laser stripes and I-Sce-I lesions; AB-G, AS and AM performed the SMARD analyses; AW, EP and PVV performed research. AAF conceived and designed the project, analyzed data with JG and AM and wrote the manuscript with SA and ADSA.

Non-author contributions and disclosures: No;

Agreement to Share Publication-Related Data and Data Sharing Statement: ChIP sequencing data is available in Gene Expression Omnibus (GEO): GSE152292 All additional data, reagents and protocols are available to other investigators. Requests should be submitted by e-mail to the corresponding author.

Clinical trial registration information (if any):

Functional mapping of PHF6 complexes in chromatin remodeling, replication dynamics and DNA repair.

Silvia Alvarez[1,†], Ana C. da Silva Almeida[1,†,§], Robert Albero[1], Mayukh Biswas[1], Angelica Barreto-Galvez[2], Thomas S. Gunning[1], Anam Shaikh[2], Tomas Aparicio[1], Agnieszka Wendorff[1], Erich Piovan[3,4], Pieter Van Vlierberghe[5,6], Steven Gygi[7], Jean Gautier[1,8], Advaitha Madireddy [2], Adolfo A. Ferrando[1,9,10,11]

[1]Institute for Cancer Genetics, Columbia University, New York, NY, 10032, USA.

[2]Rutgers Cancer Institute of New Jersey, NJ, 08903, USA.

[3]UOC Immunologia e Diagnostica Molecolare Oncologica, Istituto Oncologico Veneto-IRCCS, Padova, 35128, Italy.

[4]Dipartimento di Scienze Chirurgiche, Oncologiche e Gastroenterologiche, Sezione di Oncologia, Universita' di Padova, Padova, 35128, Italy.

[5]Department of Biomolecular Medicine, Ghent University, Ghent, 9000, Belgium.

[6]Cancer Research Institute Ghent, Ghent, 9000, Belgium.

[7]Department of Cell Biology, Harvard Medical School, Boston, MA 02115, USA.

[8]Department of Genetics and Development, College of Physicians and Surgeons, Columbia University, New York, NY, USA.

[9]Department of Systems Biology, Columbia University, New York, NY, 10032, USA.

[10]Department of Pediatrics, Columbia University Irving Medical Center, New York, NY, 10032, USA.

[11]Department of Pathology and Cell Biology, Columbia University Irving Medical Center, New York, NY, 10032, USA.

[†]Equal contribution

[§]Current address: Biogen Inc., Cambridge, Massachusetts, 02142, USA.

Contact Information:

Adolfo A. Ferrando

28 Address: 1130 St. Nicholas Ave, ICRC 402, New York, NY, 10032, USA

29 Phone: 212-851-4611; FAX: 212-851-5256

30 e-mail: af2196@columbia.edu

31

32 Silvia Alvarez

33 Address: 1130 St. Nicholas Ave, ICRC 402, New York, NY, 10032, USA

34 Phone: 212-851-4611; FAX: 212-851-5256

35 e-mail: sa3358@columbia.edu

36

37 **Classification:** Biological Sciences, Cell Biology

38 **Key words:** PHF6, DNA repair, heterochromatin, satellite DNA, replicative stress, fragile site

39

Key points

- PHF6 interacts with NuRD, SWI/SNF and ISWI factors, the replication machinery and DNA repair proteins.
- PHF6 associates with heterochromatin at satellite DNA and protects genomic fragile sites from DNA damage induced genetic instability.

Abstract

The Plant Homeodomain 6 gene (*PHF6*) encodes a nucleolar and chromatin-associated leukemia tumor suppressor with proposed roles in transcription regulation. However, specific molecular mechanisms controlled by PHF6 remain rudimentarily understood. Here we show that PHF6 engages multiple nucleosome remodeling protein complexes including NuRD, SWI/SNF and ISWI factors, the replication machinery and DNA repair proteins. Moreover, following DNA damage, PHF6 localizes to sites of DNA injury and its loss impairs the resolution of DNA breaks with consequent accumulation of single- and double-stranded DNA lesions. Native chromatin immunoprecipitation sequencing analyses reveal that PHF6 specifically associates with difficult to replicate heterochromatin at satellite DNA regions enriched in Histone H3 lysine 9 trimethyl marks (H3K9me3) and single molecule locus-specific analyses identify PHF6 as an important regulator of genomic stability at fragile sites. These results extend our understanding of the molecular mechanisms controlling HSC homeostasis and leukemia transformation by placing PHF6 at the crossroads of chromatin remodeling, replicative fork dynamics and DNA repair.

Introduction

Originally identified as the causative gene of Börjesson-Forsmann-Lehman syndrome (BFLS), an X-linked neurodevelopmental disorder[1], the Plant Homeodomain 6 gene (*PHF6*), functions as an epigenetic regulator of long-term self-renewal in hematopoietic stem cells frequently mutated in T-cell acute lymphoblastic leukemia (T-ALL), in T-myeloid mixed lineage tumors, and also, albeit less frequently, in acute myeloid leukemia and myelodisplastic syndromes[2-5]. Functionally, PHF6 localizes to the nucleolus and interacts with the PAF1 transcription elongation complex[6] implicated in the control of RNA Polymerase I activity and ribosomal DNA (rDNA) transcription and with UBF[7], a transcriptional activator in the RNA Pol I pre-initiation complex, supporting a role for PHF6 in the control of ribosome biogenesis. Moreover, PHF6 associates with the Nucleosome Remodeling Deacetylase (NuRD) complex[8], a major chromatin regulator controlling nucleosome positioning and transcription with important roles in development, genome integrity and cell cycle progression[9,10]. Finally, early and recent work on the characterization of factors involved in the clearance of γ-H2AX following DNA damage revealed that supression of PHF6 expression can impair the clearance of this DNA damage-associated mark[11,12]. Consistently, PHF6 inactivation results in γ-H2AX accumulation[3] indicating a potential link between PHF6 function and maintenance of genomic integrity[3,12].

Mechanistically, increased self renewal in the hematopoietic stem cell compartment seems to be a major effector contributing to leukemia development following *PHF6* loss[13-15]. Thus, genetic inactivation of *Phf6* primes hematopoietic stem cells to transformation by oncogenic NOTCH1 in mice and secondary loss of *Phf6* in NOTCH1-induced T-ALL increases the numbers of self-renewing leukemia initiating cells[13]. Consistently, *PHF6* mutations are recurrently found in clonal hematopoiesis associated with aging[16] and in clonal hematopoiesis developing in aplastic anemia patients as they recover from bone marrow failure[17]. In agreement, loss of *PHF6* is frequently an early initiating event in leukemia transformation[13,18]. Molecularly, *Phf6* inactivation seems to favor increased chromatin accessibility in hematopoietic stem cells and leads to the upregulation of JAK-STAT target genes[13]. In addition, loss of

Phf6 causes the upregulation of expression of gene-sets linked with increased leukemia stem cell activity[13]. However, the molecular mechanisms underlying its tumor supressor activity remain unknown. To bridge this gap, we sought to gain further insight into the molecular functions of PHF6 by analyzing the composition of PHF6-associated protein complexes isolated by tandem affinity purification. Our results uncover a broader and largely unanticipated role of PHF6 in chromatin regulation in association not only with the NuRD complex but also with the SWI/SNF machinery and implicate PHF6 in the control of replication fork dynamics and DNA repair specifically at difficult to replicate satellite DNA sites.

Methods

Isolation of PHF6 protein complexes by tandem affinity purification

We harvested HEK293T and Jurkat cells (2 x 10^9 cells) stably expressing PHF6-FLAG-HA and GFP and empty vector control GFP-expressing cells and extracted the cytoplasmic fraction by incubation in 20 volumes Cytosol Hypotonic Buffer A (10 mM HEPES pH 7.9, 10 mM KCl, 1.5 mM $MgCl_2$, 0.1 mM EDTA) supplemented with protease (Sigma-Aldrich, #11697498001) and phosphatase (Sigma-Aldrich, #4906845001) inhibitors for 15 minutes on ice, with occasional vortexing. We added 0.1% NP40 and isolated cell nuclei by centrifugation at 100 g for 15 minutes. We washed nuclear pellets once in Cytosol Hypotonic Buffer A and resuspended them in 5 volumes Nuclear Extraction Buffer C (20 mM HEPES ,pH 7.9, 400 mM NaCl, 1.5 mM $MgCl_2$, 0.4% Triton X-100, 1 mM EDTA) supplemented with protease and phosphatase inhibitors. After incubation on ice for 60 min, with frequent vortexing, we centrifuged nuclear extracts at 2000 g for 30 minutes and collected the high salt nuclear fraction supernatants and adjusted to reduce the NaCl concentration to 150-200 mM by adding Equilibration Buffer (20 mM HEPES, pH 7.9, 10% Glycerol, 1mM EDTA) supplemented with protease and phosphatase inhibitors. To immunoprecipitate PHF6-Flag-HA-containing protein complexes we incubated nuclear extracts with anti-Flag M2 beads (Sigma-Aldrich, #M8823) overnight at 4°C. We washed beads three times with PBS supplemented with protease and phosphatase inhibitors at 4ºC, and eluted protein complexes by overnight incubation in 150 mM NaCl Equilibration Buffer containing 1

mg ml^{-1} Flag peptide (Sigma-Aldrich, #F3290). We performed a second round of immunoprecipitation with anti-HA beads (ThermoFisher Scientific, #26182) as before and eluted with HA peptide (Sigma-Aldrich, #I2149). Pulled down proteins were analyzed by mass spectrometry at the Taplin Biological Mass Spectrometry Facility.

PHF6 native chromatin immunoprecipitation

We harvested 20 million cells per condition and resuspended at 10 million cells per ml of 0.3 % Triton X-100 / PBS supplemented with protease and phosphatase inhibitors to isolate nuclei. We resuspended nuclei in 250 µl of EX100 buffer (10 mM HEPES [pH 7.6], 100 mM NaCl, 1.5 mM $MgCl_2$, 0.5 mM EGTA, 10% glycerol, 0.2 mM PMSF, 1 mM DTT) and added 1.5 U μL^{-1} MNase for 20 minutes at room temperature. We stopped the reaction by adding by adding EGTA to a final concentration of 10 mM, resuspended nuclear pellets in EX100 buffer and incubated overnight at 4ºC with PHF6 (Sigma-Aldrich, #HPA001023) or IgG (Diagenode, #C15400001-15) antibodies. We used 75 µl of equilibrated magnetic beads (Sigma-Aldrich, #16-662) in EX-100 buffer for 3h at 4ºC. We washed samples twice with Wash Buffer 1 (10 mM Tris pH 7.5, 1 mM EDTA, 0.1% SDS, 0,1% sodium deoxycholate, 1% Triton X-100/H2O), once with Wash Buffer 2 (10 mM Tris pH 7.5, 1 mM EDTA, 0.1% SDS, 0,1% sodium deoxycholate, 1% Triton X-100, 150 mM NaCl / H2O) and once with 1x TE + 0.2% Triton X-100. We resuspended the samples in 100 µL of 1x TE, eluted DNA in 10% SDS + 20 mg ml^{-1} proteinase K for 1h at 65ºC and resuspended in 100 µl TE + 0.5 M NaCl. We eluted and purified DNA from input and immunoprecipitation samples using by phenol:chloroform extraction followed by ethanol precipitation, resuspended it in water and quantified by UV absorbance in a NanoDrop spectrophotometer. We used the Diagenode MicroPlex kit for Illumina platforms (Diagenode, #C05010012) following manufacturer's instructions for library preparation. We quantified the libraries using the KAPA Library Quantification Kit for Illumina Platforms (KapaBiosystems, #KR0405) and AMPure XP (Beckman, # A63880) for library purification. We sequenced amplicon pools in an Illumina NextSeq500/550. Data is available in Gene Expression Omnibus (GEO accession number: GSE152292).

Single molecule analysis of replicated DNA (SMARD)

We carried out SMARD analysis using a procedure described previously[19,20] and described in detail in the Supplemental Methods.

Statistical analyses.

Statistical analysis was performed using GraphPad Prism software v5.0 (GraphPad Software, La Jolla, CA, USA). We assumed normality and equal distribution of variance between groups, and we considered results with Student's t test $P < 0.05$ as statistically significant. Replication fiber analyses were conducted on blinded images.

Results

PHF6 prominently interacts with nucleosome remodeling protein complexes, the replication machinery and DNA repair factors.

To gain insight on the molecular mechanisms engaged in the tumor suppressor activity of PHF6 in human leukemia and general functions controlled by PHF6 we performed mass spectrometry analysis of PHF6-HA-FLAG protein complexes isolated from Jurkat, a *PHF6* wild type T-ALL cell line, and in HEK293T cells, a human fetal kidney derived cell line. These analyses revealed fundamentally overlapping protein interactions in support of a general role for PHF6 in cellular homeostasis. Across both datasets we identified 85 PHF6-associated factors (**Figure 1A-E, and supplemental Table 1**), inclusive of known PHF6 interacting proteins such as multiple members of the NuRD complex (CHD4, HDAC1, HDAC2, RBBP4, RBBP7, MBD2, MTA2, MBD3, GATAD2B). In addition, PHF6 also associated with the SWI/SNF family of chromatin remodelers in our tandem affinity purification profiling (SMARCA4, SMARCB1, SMARCC1, SMARCC2, SMARCE1) and also by co-immunoprecipitation and Western blot analyses (SMARCA4/BRG1, ARID2, BRD7, SMARCA5/SNF2H, BCL11B, WDR5, ASH2L, HCFC1 and SETD1A) (**supplemental Figure 1A-D**) suggesting a broader and more complex role of PHF6 in chromatin remodeling and nucleosome repositioning than previously recognized[21]. Indeed, functional annotation of PHF6 protein complexes revealed striking enrichment in factors involved chromatin organization ($P = 2.18^{-16}$) and epigenetic regulation of gene expression ($P = 2.23^{-15}$) (**Figure**

1A-E, and supplemental Table 2). Moreover, and in agreement with the proposed roles of PHF6 in chromatin remodeling and control of rRNA transcription, PHF6-associated factors prominently included epigenetic regulators involved in control of rRNA expression (P= 5.13^{-16}) and proteins involved in RNA Polymerase I-mediated transcriptional regulation (P= 6.82^{-14}) (**Figure 1E**). Finally, the PHF6 interactome also included numerous factors involved in chromosome maintenance (P= 3.1^{-5}) and DNA repair (P= 3.21^{-4}) as well as proteins controlling cell cycle and DNA synthesis (P= 4.80^{-5}) (**Figure 1D**).

PHF6 is a DNA repair factor recruited to double-strand breaks

PHF6 inactivation can lead to acumulation of the γ-H2AX DNA-damage marker[3,11,12], increased replication-transcription conflicts at ribosomal DNA sites[7], and delayed DNA repair[22]. To explore the relationship between PHF6 and the DNA damage response we tested whether PHF6 could be recruited to DNA damage sites. Notably, immunofluorescence analysis showed that PHF6 protein relocated to laser-generated stripes marked by γ-H2AX just 5 min after microirradiation pointing to a role of PHF6 as an early repair factor (**Figure 2A**). Similarly, immunofluorescence (**Figure 2B**) and chromatin immunoprecipitation assays (**Figure 2C**) documented the recruitment of PHF6 to a single- double-stranded DNA break generated by the I-*Sce*I restriction enzyme in U2OS cells that faded away when moving away from the break site indicating a specific binding of PHF6 to the break site. Next, we assessed the impact of PHF6 knockdown on the efficacy of homologous-recombination, single-strand annealing and non-homologous end-joining DNA repair pathways with specific GFP reporters[23] in U2OS cells. In these analyses, PHF6 knockdown resulted in a highly significant decrease in both homologous-recombination and single-strand annealing double-strand break repair compared to control cells and a more moderate, yet significant, reduction in the efficiency of non-homologous end-joining (**Figure 2D, supplemental Figure 2A-B**), which implicates PHF6 in the resolution of single- and double-strand breaks. To gain mechanistic insights on the different repair pathways in which PHF6 was involved, we transiently treated PHF6 knockdown and control cells with neocarzinostatin, a radiomimetic DNA-damaging agent and performed immunofluorescence assays of different players in recombination dependent or independent repair. We first addressed the level and nuclear localization of

BRCA1, the main factor promoting resection in homologous recombination repair[24] and Rad51, a key player in crossover regulation[25]. To evaluate the initial steps of non-homologous end joining in PHF6-deficient cells we checked the levels of Ku80, the main double-stranded break sensor and of XRCC4, which promotes the religation or broken ends and serves as an activity readout for the main NHEJ kinase, DNA-PK[26]. Although we did not observe any major differences in the number or intensity of Ku80 or XRCC4 foci (**supplemental Figure 2C**) we found a clear persistence of Rad51 foci after 6h of recovery indicating a failure in resolving DNA damage downstream resection or at the level of homologous strand search (**Figure 2E-F**). We did not observe a different intensity of BRCA1 foci, indicating that PHF6 loss does not impact on the global levels of BRCA1. However, and as reported before in the case of a low dose of irradiation[27], we observe BRCA1 nuclear export after the induction of DNA damage. Interestingly, PHF6-deficient cells showed an earlier cytoplasmic BRCA1 signal soon after treatment, suggesting that PHF6 could be necessary for BRCA1 nuclear retention (**supplemental Figure 2D**). This premature BRCA1 export in PHF6-deficient cells could contribute to the observed defects in homologous recombination. Following on these results, we monitored and quantified the resolution of single- and double-strand DNA breaks visualized by alkaline comet assay. PHF6 depletion resulted in delayed resolution of both types of breaks over time (**Figure 2G-H**), which was in line with the impaired resolution of Rad51 foci, suggesting a functional role for PHF6 in recombination-mediated repair. Consistently, we observed a more rapid and persistent increase in γH2AX levels in Phf6 deficient primary NOTCH1-induced leukemic lymphoblasts compared with their isogenic controls (**Figure 2I**). Ultimately, the loss of PHF6 led to increased apoptosis in *PHF6*-deficient cells after gamma irradiation and after a high-dose of hydroxyurea, indicating that PHF6 loss can promote DNA damage induced apoptosis (**Figure 2J, supplemental Figure 2E-I**). Importantly, we did not observe increased apoptosis outside highly genotoxic conditions. Specifically, low amounts of replication stress as induced by sustained low dose hydroxyurea treatment did not result in increased apoptosis in PHF6 knockdown cells (**supplemental Figure 2G**). The association of PHF6 with both chromatin remodeling complexes and with the replication and DNA repair machinery suggested a potential role for PHF6 in the

epigenetic control of DNA repair. To formally test this hypothesis we evaluated the recruitment of the chromatin remodeling factors CHD4 and SMARCB1 to a single DNA damage site induced by I-*Sce*I in wild type or PHF6-deficient cells. Interestingly, CHD4 recruitment to a unique DNA damage site was significantly impaired upon PHF6 loss while a similar trend was observed in the recruitment of SMARCB1 (**Figure 2K-L, supplemental Figure 2J-K**) suggesting that PHF6 creates an adequate chromatin environment needed for its DNA repair functions. To further investigate the interaction between PHF6-associated epigenetic regulators and the DNA damage response we evaluated the effects of neocarzinostatin treatment in the interaction of PHF6 with different chromatin remodelers. These experiments revealed increased PHF6-SMARCA5/SNF2H interaction in response to DNA damage, while no changes in the PHF6 bound fraction to NuRD or SWI/SNF chromatin remodelers was observed (**Figure 2M, supplemental Figure 2L-M**). These results support a potential role for CHD4/PHF6 and SMARCA5/SNF2H-PHF6 complexes in providing an adequate chromatin environment during DNA damage. Interestingly, SMARCA5/SNF2H accumulates on nascent DNA upon replication-associated damage[28] while CHD4 loss promotes increased replication fork stability increasing the chemoresistance of homologous recombination deficient cells[29], data that places these two chromatin remodelers as important responders against replication stress. To further understand the mechanisms of DNA repair, replication and PHF6 regulation, we performed mass spectrometry-based phosphoproteomic analysis of PHF6 protein immunoprecipitated from neocarzinostatin-treated HEK293T cells[30] and we assessed whether PHF6 was a target of the DNA damage response kinases. We identified five damage-dependent phosphorylation sites in PHF6 (S120, S138, S155, S199 and S204), three of which (S120, S199 and S204) were suppressed by treatment with caffeine, an inhibitor of phosphatidylinositol 3-kinase-related kinase kinases (ATR, PRKDC/DNA-PK and ATM) (**supplemental Figure 2N**). Furthermore, western-blot analysis of HEK293T Flag-HA-PHF6 immunoprecipitates demonstrated increased immunoreactivity with an antibody recognizing the ATM/ATR DNA phosphorylation motif following γ-radiation (**supplemental Figure 2O**). Taken together, these results implicate PHF6 as a DNA repair factor recruited to double strand breaks and

phosphorylated by DNA repair signaling kinases. Moreover, the presence of PHF6 in complex with factors involved in the control of cell cycle and DNA synthesis (**Figure 1D**) suggests a potential role for PHF6 in DNA homeostasis in association with the DNA replication machinery.

PHF6 protects replication fork integrity by regulating the speed of DNA synthesis.

To formally evaluate this possibility, we performed DNA fiber analysis to document replication fork dynamics[31] in *PHF6* wild type and knockout cells after sequential labeling of nascent DNA with chlorodeoxyuridine (CldU, red) and iododeoxyuridine (IdU, green). CUTLL1 *PHF6* and Jurkat *PHF6* knockout T-ALL leukemia cells showed a significant increase in IdU (green) and CldU (red) DNA track lengths compared with isogenic *PHF6* wild type controls (**Figure 3A, B** and **supplemental Figure 3A**), indicative of accelerated replication fork progression. In addition, we noted increased replication fork pausing, demonstrated by asymmetric DNA fibers, in *PHF6* knock-out cells compared with controls (**Figure 3C** and **supplemental Figure 3B-C**), which is consistent with increased genomic instability in the context of accelerated DNA replication[32]. PHF6 interacts with the UBF transcription factor in the nucleolus, which contributes to downregulate rDNA transcription and to prevent rDNA damage[7]. The observed increase in replication fork progression upon PHF6 loss in association with upregulation of rDNA transcription may explain the observation of an increase in collapsed replication forks and double-strand DNA breaks or R-loop DNA-RNA hybrids at rDNA sites after PHF6 inactivation[7]. To determine if the loss of PHF6 could also exacerbate the formation of R-loops in the presence of replication stress, we treated wild type or PHF6-deficient cells with hydroxyurea and/or and ATR inhibitor. These experiments revealed an increase in the number of R-loops in PHF6-deficient cells under replication stress, further supporting a role in the resolution of DNA-RNA hybrids (**supplemental Figure 3D-E**).

The RPA DNA repair factor is progressively phosphorylated by ATR at Ser33 at replication-associated DNA double-strand breaks to promote DNA repair[33] and specifically functions as a rate limiting factor shielding replication forks from collapse [34]. To further explore the role of PHF6 in the sensing and resolution of DNA damage we analyzed the effect of PHF6 inactivation in the induction of RPA Ser33

phosphorylation after treatment with the replication stress-inducing agent camptothecin (**Figure 3D**). In this setting, PHF6 inactivation resulted in decreased RPA S33 phosphorylation in agreement with a defective replicative stress response. ATR phosphorylation at T1989 is required for ATR activation upon replication associated DSBs[35] upstream of RPA S33 phosphorylation. Notably, we observed increased ATR T1989 phosphorylation in PHF6 knockout cells under different replication stress conditions (camptothecin and neocarzinostatin treatment) (**supplemental Figure 3F-G**). As PHF6 knockout cells display a reduced RPA S33 phosphorylation (with increased ATR pT1989), we conclude that PHF6 is necessary for the phosphorylation of RPA by activated ATR. Altogether, these results implicate PHF6 in the preservation of replication fork integrity.

To gain a better understanding of the role of PHF6 across the chromatin landscape we performed chromatin immunoprecipitation followed by deep sequencing (ChIP-Seq) in native chromatin from in T-ALL lymphoblast cells. These analyses revealed that PHF6 was specifically enriched at genomic locations corresponding to H3K9me3 domains in Jurkat cells, but not in *PHF6* knockout controls (**Figure 3E and supplemental Figure 4A-B**). H3K9me3 marks heterochromatic regions, which in the human genome primarily correspond to genomic areas with high copy number tandem repeat sequences including satellite repeat and transposon regions[36]. Analysis of the distribution of PHF6 ChIP-Seq signals across different heterochromatin domains revealed a marked overlap between PHF6 occupancy and satellite DNA regions (**Figure 3F**), a feature readily noticeable in the large satellite heterochromatin areas of human chromosome 19 (**Figure 3E** and **supplemental Figure 4C**). Notably, satellite DNA poses a major challenge for the DNA replication machinery resulting in increased replication fork stalling, which can lead to chromosomal breaks and rearrangements [37].

The functional requirement of PHF6 for efficient DNA repair, its association with chromatin remodeling factors, and its localization to satellite DNA domains support a role in chromatin dynamics during DNA replication and in the maintenance of genomic integrity. Consistently, even though PHF6-containing chromatin in untreated conditions showed limited overlap with γ-H2AX, we observed a high overlap between non-treated PHF6-containing regions and aphidicolin treated γ-H2AX domains (P = 0.001)

supporting the idea that PHF6 pre-occupies difficult-to-replicate DNA regions, which are revealed upon replication stress (**Figure 3G, H**). Indeed, PHF6 was markedly enriched at the common fragile site FRA3H, a common fragile site induced by aphidicolin in the human genome[38] that appears as a hotspot of replicative stress marked by high levels of γ-H2AX following aphidicolin treatment (**Figure 3I**). Altogether, these observations indicate that PHF6 is likely recruited to fragile genomic regions, which are highly susceptible to replicative stress-induced DNA damage, where it could facilitate DNA replication and repair to maintain genomic integrity. To test this hypothesis, we analyzed the impact of PHF6 loss at common fragile sites as these hypermutable repetitive loci are highly susceptible to replicative stress-induced DNA damage[39] and represent common hotspots for chromosomal rearrangements in human cancer[40]. Single-molecule analysis of replicated DNA (SMARD)[20] at the FRA16D fragile site (**Figure 4A**) showed that replication proceeds predominantly in the 3' to 5' direction, with limited fork stalling in PHF6 wild type cells (**Figure 4B**), a pattern consistent with that reported in B cells[20]. In contrast, analysis of *PHF6* knock-out cells revealed an increase in the number of stalled replication forks at this locus (**Figure 4B**), as well as extended DNA frament lengths and abnormal FISH probe patterns indicative of accumulating genomic rearrangements (**Figure 4B,C**). These results implicate PHF6 in the maintenance of genomic integrity and more specifically in the protection of difficult to replicate heterochromatin-associated fragile sites.

Discussion

Nucleosome remodeling complexes play an essential role in creating a dynamic environment where chromatin can be accesible for DNA replication and repair[39,41-43]. However the mechanisms that coordinate chromatin reorganization with the DNA synthesis and repair machinery and the role of chromatin remodeling DNA-repair interactions in the pathogenesis of cancer remain poorly understood.

Nucleosome displacement in the context of DNA damage and repair may comprise diverse nucleosome remodeling complexes involved both in increasing chromatin accessibility (SWI/SNF) and in favoring a closed chromatin configuration (NuRD). In addition, local monoubiquitylation of H2BK120 at double-strand DNA breaks promotes increased chromatin accessibility by SMARCA5 SWI/SNF complexes to

facilitate efficient recruitment of factors involved in homologous recombination, in support of a functional interaction between histone marks and nucleosome repositioning in DNA repair[44,45]. Interestingly, a recent report has proposed a dual role for PHF6 as a epigenetic reader of H2BK12 acetylation and as a epigenetic writer for histone H2BK120 ubiquitination of functional relevance for regulation of trophectodermal gene expression[46]. A prominent finding reported here is the increased interaction between PHF6 and SMARCA5 following induction of DNA damage. SMARCA5, the central component of the mammalian ISWI family of chromatin remodelers is actively involved in regulating chromatin structure and in this role facilitates the efficient recruitment of DNA repair factors[21]. Following DNA damage SMARCA5 is actively recruited to break sites through PARP1[47] and in addition, it can be found enriched at active elongating replication forks[48] where it enables replication through highly heterochromatic regions[49]. The role of PHF6 in restraining rRNA expression[7] together with our observation of increased replication fork progression is consistent with the documented increase in collapsed replication forks due to the presence of DNA-RNA hybrids in the nucleolus after PFH6 inactivation[7]. However, the role of PHF6 in maintenance of genomic integrity does not seem to be restricted to rDNA loci. Indeed, PHF6 is actively recruited to sites of DNA double-strand break and associates with numerous factors involved in chromosome maintenance and DNA repair suggesting a more general role in genomic integrity. Moreover, we observed a particularly prominent overlap between PHF6 pre-occupied genomic locations and sites of DNA damage marked by γ-H2AX upon induction of replicative stress. The location of PHF6 at sites of replicative stress-induced DNA damage could well correspond with its proposed role in the maintenance of genomic integrity, as resolution of R-loops and replication fork collapse events involves both active assembly of DNA repair complexes and active chromatin remodeling. However, the association of PHF6 with protein complexes directly involved in controlling cell cycle and DNA synthesis suggests a more direct link with the replication machinery.

The rDNA loci are composed of multiple sequence repeats in tandem, which represents a particular challenge for the replication machinery. However, most highly repetitive sequence domains in the

genome correspond to satellite DNA heterochromatin regions marked by the H3K9me3 histone mark[36]. Cancer genome studies have revealed that mutations accumulate at much higher levels in compact, H3K9me3-rich heterochromatin domains[50], consistent with the slower rates of DNA repair reported in heterochromatin[51,52]. Remarkably, we observed a prominent overlap between PHF6 occupancy and satellite DNA domains, arguing for a broader functional role of PHF6 in preventing and resolving replication fork stalling at difficult to replicate DNA sites beyond rDNA repeats. This hypothesis is further supported by our single molecule locus-specific analysis of replication dynamics and genomic integrity at the FRA16D fragile site, which revealed increased numbers of stalled replication forks and accumulating genomic rearrangements. Our results unravel a discrete and distinct role for PHF6 in the maintenance of genomic integrity by limiting replication fork dynamics particularly in difficult to replicate satellite DNA regions, but also by active recruitment to sites of double-strand DNA break where it facilitates the resolution of DNA damage. We propose that PHF6 has a local effect at repetitive regions conducive of fork stalling that can result in the observed global increase in replication fork progression and asymmetric forks. While a functional role for PHF6 in non-homologous end joining has been recently proposed[12], we observed broader defects in DNA repair implicating PHF6 also in homologous recombination and single-strand anealing. A more general role of PHF6 in resolution of DNA damage is consistent with its participation in DNA repair functions in concert with the recruitment of nucleosome remodeling factors required to facilitate access to damage sites. Alternatively, it is also possible that PHF6 participates in different forms of DNA repair via association with distinct chromatin remodeling complexes.

Leukemia-focused and pan-cancer mutational profiling analyses have established a specific tumor suppressor role for PHF6 in the hematopoietic compartment. This activity, seems to be functionally linked to an increased stem cell self-renewal and sensitization to NOTCH1 induced transformation[13]. However, the identification of a PHF6 function in the control of replicative dynamics and DNA repair suggests that defects in PHF6 could also favor leukemia transformation by accelerating the accumulation of DNA damage with consequent accumulation of secondary genetic alterations in

oncogenes and tumor suppressor genes. In an analogous way genes associated with DNA repair, DNA ligase IV and Fanconi DNA repair factor gene mutations result in abrogation of self-renewal in the hematopoietic system and cause bone marrow aplasia while at the same time favoring leukemia development as a result of increased genomic instability[53,54]. An intriguing possibility that warrants further studies is that loss of PHF6 could associate with collateral vulnerabilities that could be exploited therapeutically in the treatment of human leukemia.

Acknowledgements and funding sources

This work was supported by the National Institutes of Health grants R35 CA210065 (AF), R01AG077020 (AF), R01 CA155743 (AF), and P30 CA013696 (in support of the Herbert Irving comprehensive Cancer Center Genomics, Flow Cytometry and Molecular Cytogenetics, Genetically Manipulated Mouse Models, Proteomics and Macromolecular Crystallography, Genomics and High Throughput Screen Shared Resource, and Confocal and Specialized Microscopy Shared Resources). AAW was supported by a Rally Foundation fellowship. PvV was supported by the Fund for Scientific Research (FWO) Flanders (postdoctoral fellowship and Odysseus type 2 grant). SA was supported by a Leukemia and Lymphoma Society Special Fellowship Award. RA was supported by a Leukemia and Lymphoma Society Fellowship Award. We thank Dr. Jeremy Stark for U2OS-EJ5-GFP and U2OS SA-GFP cells.

Author contributions

SA and ADSA performed most of the experiments; RA and MB analyzed the ChIP-Seq data; SG analyzed mass-spectrometry data; TA performed immunostainings on laser stripes and I-*Sce-I* lesions; AB-G, AS and AM performed the SMARD analyses; AW, EP and PVV performed research. AAF conceived and designed the project, analyzed data with JG and AM and wrote the manuscript with SA and ADSA.

References

1. Jahani-Asl A, Cheng C, Zhang C, Bonni A. Pathogenesis of Börjeson-Forssman-Lehmann syndrome: Insights from PHF6 function. *Neurobiol Dis*. 2016;96:227-235.

2. Todd MA, Ivanochko D, Picketts DJ. PHF6 Degrees of Separation: The Multifaceted Roles of a Chromatin Adaptor Protein. *Genes (Basel)*. 2015;6(2):325-352.

3. Van Vlierberghe P, Palomero T, Khiabanian H, et al. PHF6 mutations in T-cell acute lymphoblastic leukemia. *Nat Genet*. 2010;42(4):338-342.

4. Van Vlierberghe P, Patel J, Abdel-Wahab O, et al. PHF6 mutations in adult acute myeloid leukemia. *Leukemia*. 2011;25(1):130-134.

5. Alexander TB, Gu Z, Iacobucci I, et al. The genetic basis and cell of origin of mixed phenotype acute leukaemia. *Nature*. 2018;562(7727):373-379.

6. Zhang C, Mejia LA, Huang J, et al. The X-linked intellectual disability protein PHF6 associates with the PAF1 complex and regulates neuronal migration in the mammalian brain. *Neuron*. 2013;78(6):986-993.

7. Wang J, Leung JW, Gong Z, Feng L, Shi X, Chen J. PHF6 regulates cell cycle progression by suppressing ribosomal RNA synthesis. *J Biol Chem*. 2013;288(5):3174-3183.

8. Todd MAM, Picketts DJ. PHF6 Interacts with the Nucleosome Remodeling and Deacetylation (NuRD) Complex. *Journal of Proteome Research*. 2012;11(8):4326-4337.

9. Gursoy-Yuzugullu O, House N, Price BD. Patching Broken DNA: Nucleosome Dynamics and the Repair of DNA Breaks. *J Mol Biol*. 2016;428(9 Pt B):1846-1860.

10. Li DQ, Yang Y, Kumar R. MTA family of proteins in DNA damage response: mechanistic insights and potential applications. *Cancer Metastasis Rev*. 2014;33(4):993-1000.

11. Matsuoka S, Ballif BA, Smogorzewska A, et al. ATM and ATR substrate analysis reveals extensive protein networks responsive to DNA damage. *Science*. 2007;316(5828):1160-1166.

12. Warmerdam DlO, Alonso-de Vega I, Wiegant WW, et al. PHF6 promotes non-homologous end joining and G2 checkpoint recovery. *EMBO reports*. 2020;21(1):e48460.

13. Wendorff AA, Quinn SA, Rashkovan M, et al. Phf6 Loss Enhances HSC Self-Renewal Driving Tumor Initiation and Leukemia Stem Cell Activity in T-ALL. *Cancer Discov*. 2019;9(3):436-451.

14. Miyagi S, Sroczynska P, Kato Y, et al. The chromatin-binding protein Phf6 restricts the self-renewal of hematopoietic stem cells. *Blood*. 2019;133(23):2495-2506.

15. Hsu YC, Chen TC, Lin CC, et al. Phf6-null hematopoietic stem cells have enhanced self-renewal capacity and oncogenic potentials. *Blood Adv*. 2019;3(15):2355-2367.

16. Abelson S, Collord G, Ng SWK, et al. Prediction of acute myeloid leukaemia risk in healthy individuals. *Nature*. 2018;559(7714):400-404.

17. Yoshizato T, Dumitriu B, Hosokawa K, et al. Somatic Mutations and Clonal Hematopoiesis in Aplastic Anemia. *N Engl J Med*. 2015;373(1):35-47.

18. Xiao W, Bharadwaj M, Levine M, et al. PHF6 and DNMT3A mutations are enriched in distinct subgroups of mixed phenotype acute leukemia with T-lineage differentiation. *Blood Adv*. 2018;2(23):3526-3539.

19. Norio P, Schildkraut CL. Visualization of DNA Replication on Individual Epstein-Barr Virus Episomes. 2001;294(5550):2361-2364.

20. Madireddy A, Kosiyatrakul Settapong T, Boisvert Rebecca A, et al. FANCD2 Facilitates Replication through Common Fragile Sites. *Molecular Cell*. 2016;64(2):388-404.

21. Aydin ÖZ, Vermeulen W, Lans H. ISWI chromatin remodeling complexes in the DNA damage response. *Cell Cycle*. 2014;13(19):3016-3025.

22. Warmerdam DO, Alonso-de Vega I, Wiegant WW, et al. PHF6 promotes non-homologous end joining and G2 checkpoint recovery. *EMBO reports*. 2020;21(1):e48460.

23. Gunn A, Stark JM. I-SceI-based assays to examine distinct repair outcomes of mammalian chromosomal double strand breaks. *Methods Mol Biol*. 2012;920:379-391.

24. Huen MS, Sy SM, Chen J. BRCA1 and its toolbox for the maintenance of genome integrity. *Nat Rev Mol Cell Biol*. 2010;11(2):138-148.

445 25. West SC. Molecular views of recombination proteins and their control. *Nat Rev Mol Cell Biol*.
446 2003;4(6):435-445.
447 26. Mahaney BL, Meek K, Lees-Miller SP. Repair of ionizing radiation-induced DNA double-strand
448 breaks by non-homologous end-joining. *Biochem J*. 2009;417(3):639-650.
449 27. Feng Z, Kachnic L, Zhang J, Powell SN, Xia F. DNA damage induces p53-dependent BRCA1
450 nuclear export. *J Biol Chem*. 2004;279(27):28574-28584.
451 28. Ribeyre C, Zellweger R, Chauvin M, et al. Nascent DNA Proteomics Reveals a Chromatin
452 Remodeler Required for Topoisomerase I Loading at Replication Forks. *Cell Reports*. 2016;15(2):300-
453 309.
454 29. Ray Chaudhuri A, Callen E, Ding X, et al. Replication fork stability confers chemoresistance in
455 BRCA-deficient cells. *Nature*. 2016;535(7612):382-387.
456 30. Cozzarelli NR. The mechanism of action of inhibitors of DNA synthesis. *Annu Rev Biochem*.
457 1977;46:641-668.
458 31. Nieminuszczy J, Schwab RA, Niedzwiedz W. The DNA fibre technique – tracking helicases at
459 work. *Methods*. 2016;108:92-98.
460 32. Maya-Mendoza A, Moudry P, Merchut-Maya JM, Lee M, Strauss R, Bartek J. High speed of fork
461 progression induces DNA replication stress and genomic instability. *Nature*. 2018;559(7713):279-284.
462 33. Shiotani B, Nguyen HD, H√•kansson P, et al. Two distinct modes of ATR activation orchestrated
463 by Rad17 and Nbs1. *Cell reports*. 2013;3(5):1651-1662.
464 34. Toledo Luis I, Altmeyer M, Rask M-B, et al. ATR Prohibits Replication Catastrophe by
465 Preventing Global Exhaustion of RPA. *Cell*. 2013;155(5):1088-1103.
466 35. Liu S, Shiotani B, Lahiri M, et al. ATR autophosphorylation as a molecular switch for checkpoint
467 activation. *Molecular cell*. 2011;43(2):192-202.
468 36. Janssen A, Colmenares SU, Karpen GH. Heterochromatin: Guardian of the Genome. *Annu Rev*
469 *Cell Dev Biol*. 2018;34:265-288.

37. Madireddy A, Gerhardt J. Replication Through Repetitive DNA Elements and Their Role in Human Diseases. In: Masai H, Foiani M, eds. DNA Replication: From Old Principles to New Discoveries. Singapore: Springer Singapore; 2017:549-581.

38. Filipović J, Joksić G, Vujić D, et al. First molecular-cytogenetic characterization of Fanconi anemia fragile sites in primary lymphocytes of FA-D2 patients in different stages of the disease. *Mol Cytogenet*. 2016;9(1):70.

39. Glover TW, Wilson TE, Arlt MF. Fragile sites in cancer: more than meets the eye. *Nature Reviews Cancer*. 2017;17:489.

40. Dillon LW, Burrow AA, Wang Y-H. DNA instability at chromosomal fragile sites in cancer. *Current genomics*. 2010;11(5):326-337.

41. Soria G, Polo SE, Almouzni G. Prime, repair, restore: the active role of chromatin in the DNA damage response. *Mol Cell*. 2012;46(6):722-734.

42. Smerdon MJ. DNA repair and the role of chromatin structure. *Curr Opin Cell Biol*. 1991;3(3):422-428.

43. Rother Magdalena B, van Attikum H. DNA repair goes hip-hop: SMARCA and CHD chromatin remodellers join the break dance. *Philosophical Transactions of the Royal Society B: Biological Sciences*. 2017;372(1731):20160285.

44. Moyal L, Lerenthal Y, Gana-Weisz M, et al. Requirement of ATM-dependent monoubiquitylation of histone H2B for timely repair of DNA double-strand breaks. *Mol Cell*. 2011;41(5):529-542.

45. Nakamura K, Kato A, Kobayashi J, et al. Regulation of homologous recombination by RNF20-dependent H2B ubiquitination. *Mol Cell*. 2011;41(5):515-528.

46. Oh S, Boo K, Kim J, et al. The chromatin-binding protein PHF6 functions as an E3 ubiquitin ligase of H2BK120 via H2BK12Ac recognition for activation of trophectodermal genes. *Nucleic Acids Res*. 2020;48(16):9037-9052.

494 47. Smeenk G, Wiegant WW, Marteijn JA, et al. Poly(ADP-ribosyl)ation links the chromatin
495 remodeler SMARCA5/SNF2H to RNF168-dependent DNA damage signaling. *J Cell Sci*. 2013;126(Pt
496 4):889-903.
497 48. Sirbu BM, McDonald WH, Dungrawala H, et al. Identification of proteins at active, stalled, and
498 collapsed replication forks using isolation of proteins on nascent DNA (iPOND) coupled with mass
499 spectrometry. *J Biol Chem*. 2013;288(44):31458-31467.
500 49. Collins N, Poot RA, Kukimoto I, Garc√≠a-Jim√©nez C, Dellaire G, Varga-Weisz PD. An ACF1-
501 ISWI chromatin-remodeling complex is required for DNA replication through heterochromatin. *Nat*
502 *Genet*. 2002;32(4):627-632.
503 50. Schuster-Böckler B, Lehner B. Chromatin organization is a major influence on regional mutation
504 rates in human cancer cells. *Nature*. 2012;488(7412):504-507.
505 51. Goodarzi AA, Kurka T, Jeggo PA. KAP-1 phosphorylation regulates CHD3 nucleosome
506 remodeling during the DNA double-strand break response. *Nat Struct Mol Biol*. 2011;18(7):831-839.
507 52. Noon AT, Shibata A, Rief N, et al. 53BP1-dependent robust localized KAP-1 phosphorylation is
508 essential for heterochromatic DNA double-strand break repair. *Nat Cell Biol*. 2010;12(2):177-184.
509 53. Ceccaldi R, Parmar K, Mouly E, et al. Bone marrow failure in Fanconi anemia is triggered by an
510 exacerbated p53/p21 DNA damage response that impairs hematopoietic stem and progenitor cells. *Cell*
511 *stem cell*. 2012;11(1):36-49.
512 54. Murray JE, Bicknell LS, Yigit G, et al. Extreme Growth Failure is a Common Presentation of
513 Ligase IV Deficiency. *Human Mutation*. 2014;35(1):76-85.

514

515

Figures and Figure Legends

Figure 1. PHF6 associates with protein complexes involved in chromatin regulation and DNA repair. A, Purified proteins after tandem affinity purification visualized by silver staining. Molecular weight marker (MW marker) is indicated on the left. **B,** ConsensusPathDB over-representation analysis of protein complexes. **C,** ConsensusPathDB over-representation analysis showing enrichment in chromatin remodeling pathways. **D,** ConsensusPathDB over-representation analysis showing enrichment in DNA repair pathways. **E,** ConsensusPathDB over-representation analysis showing enrichment in rRNA expression regulation pathways.

Figure 2. PHF6 is recruited to the vicinity of DNA breaks and for efficient DNA repair. A, Representative confocal images showing PHF6 co-localization with γ-H2AX after UV microirradiation in U2OS cells. **B**, Representative confocal images showing PHF6 co-localizing with γ-H2AX in a single double-strand break induced by I-*Sce*I expression in U2OS-DR GFP cells. **C,** Upper panel, schematics of double-strand break induction after doxycycline and PHF6 recruitment to the vicinity of a double-strand break (region A) and to two different regions away from the double-strand break (region B and C). Lower panel, quantification of chromatin immunoprecipitation assay showing PHF6 recruitment to the vicinity of the I-*Sce*I DSB site in U2OS-DR-GFP cells in 3 different genomic regions (A, B and C) in two independent experiments. Bar graphs represent mean ± SEM and p-values were assessed using two-tailed unpaired Student's t-test. **D,** GFP percentage measured by flow cytometry in U2OS cells expressing 2 different shRNAs targeting PHF6 or control shRNA containing integrated reporters to measure DNA repair efficiency through homologous recombination, (U2OS-DR-GFP), single-strand annealing (SA-GFP) or non-homologous end joining (EJ5-GFP). The percentage of GFP positive cells is plotted as percentage relative to the control cells. Data are representative of 4 independent experiments. Bar graphs represent mean ± SEM and p-values were assessed using two-tailed unpaired Student's t-test. **E,** Representative images of Rad51 foci (red) obtained after 1h or 6h recovery from

neocarzinostatin treatment. DNA was stained with DAPI (blue). Scale bar 25 μM. **F,** Quantification of the intensity of Rad51 foci (red) per cell in control and PHF6-knockout U2OS cells. Between 100 and 200 cells were analyzed per condition. Statistical analysis was conducted using a non-parametric Mann-Whittney test. Data are representative of two independent experiments. **G,** Representative alkaline comet images performed in untreated U2OS cells or after neocarzinostatin treatment (100 ng/ml) and recovery for 1h, 4h or 6h. **H,** Dot plot showing individual percentages of comet tail DNA. The median value of more than 70 nuclei per experimental condition is indicated. Statistical analysis was conducted using Mann-Whitney. Data are representative of two independent experiments. **I,** Western blot showing the presence of phosphorylated γH2AX after recovery from irradiation (1 Gy) for the indicated times in PHF6 control or knock-out primary T-ALL cells. Gapdh is shown as loading control. **J,** Analysis of apoptosis upon irradiation at 8 Gy in U2OS infected with control sgRNA or sgRNA#1/ sgRNA#2. Bar graphs represent mean ± SD and p-values were assessed using two-tailed unpaired Student's t-test. **K,** Quantification of chromatin immunoprecipitation assay showing CHD4 recruitment to the vicinity of the I-*Sce*I DSB site in U2OS-DR-GFP cells (region A) in three independent experiments. Bar graphs represent mean ± SD and p-values were assessed using two-tailed unpaired Student's t-test. **L,** Quantification of chromatin immunoprecipitation assay showing SMARCB1 recruitment to the vicinity of the I-*Sce*I DSB site in U2OS-DR-GFP cells (region A) in three independent experiments. Bar graphs represent mean ± SD and p-values were assessed using two-tailed unpaired Student's t-test. **M,** Left, Western Blot confirming endogenous PHF6 interaction by immunoprecipitation with SNF2H before and after treatment with 100 ng/ml NCS. Right, Quantification of Phf6 levels normalized to Phf6 input +/- NCS.

Figure 3. PHF6 protects from replication-associated DNA damage and binds to satellite DNA heterochromatin. A, Schematic of CldU/IdU pulse labeling (upper left). Representative images of CldU and IdU replication tracks in Jurkat control or PHF6-knock-out cells (bottom left). Fork rate dot plot

showing the IdU tract length of individual replication forks in untreated Jurkat cells (right). The median value of more than 350 tracts per experimental condition is indicated. Statistical analysis was conducted using Mann-Whitney test (**** $p < 0.0001$). Data are representative of two independent experiments. **B,** Western blot showing PHF6 knock-out in Jurkat cells expressing an sgRNA targeting the second PHD2 domain of PHF6. β-actin concentrations are shown as a loading control **C,** Left, scheme of the signals used for quantification of asymmetry analysis of forks moving from a single origin (outgoing forks). Right, scatter diagram of fork symmetry in Jurkat cells. Each dot corresponds to the ratio between the right and the left fork velocities of a pair of outgoing forks belonging to the same replication bubble. The areas outside of the dotted lines include all points whose ratios deviate from the expected theoretical value of 1 ± 0.3 corresponding to forks moving bidirectionally at nearly the same rate. Statistical analysis was done with Mann-Whitney rank sum test (***$p<0.001$). **D**, Western blot showing the presence of phosphorylated RPA after recovery from a 30 min of 1μM camptothecin treatment. '–' sign, untreated conditions. Both RPA total amount and β-actin concentrations are shown as a loading control as were used for the blot quantification shown below each band. **E**, Chromosome 19 distribution of normalized PHF6 (red track) or H3K9me3 (blue track) ChIP-seq intensities in Jurkat. **F**, Heat map indicating the logFC enrichment in repetitive regions by category compared to the average in three random subsets. **G**, Overlap between PHF6 peaks and γH2AX genomic regions in untreated (upper panel) and after aphidicolin treatment (lower panel). The indicated p-value and Z-score are the result of permutation test (n=1000 trials) **H**, Normalized ChIP-Seq heat maps of Jurkat PHF6 control and KO and K562 γH2AX aphidicolin treated and untreated. PHF6-bound regions (n=11528) were scaled to the same length. **I**, Differential PHF6 (control/KO cell lines) and γH2AX (treated/untreated) ChIP-seq intensities within the fragile site FRA3H.

Figure 4. PHF6 prevents replication-associated damage and accumulation of genomic rearrangements at the FRA16D chromosome fragile site. A, Locus map of CFS-FRA16D *Sbf*I

digested segment. The FISH probes that identify the segment are labeled in blue. **B,** Aligned photomicrograph images of labeled DNA molecules from Jurkat PHF6 empty vector or Jurkat PHF6 KO. The yellow arrows indicate the sites along the molecules where the IdU transitioned to CldU. White rectangles indicate representative sites of replication fork pausing. The molecules are arranged in the following order: molecules with initiation events, molecules with 3' to 5' progressing forks, molecules with 5' to 3' progressing forks and molecules with termination events. The quantification in the upper right panel shows the percentage of molecules with rearrangements at CFS-FRA16D in Jurkat PHF6 EV (blue bar) and Jurkat KO (red bar). Error bars represent mean ± SD from data collected from two independent experiments. The quantification in the lower right panel shows the replication fork speed at CFS-FRA16D in Jurkat PHF6 EV (blue bar) and Jurkat KO (red bar). Error bars represent mean ± SD from data collected from two independent experiments. **C,** Close up of the 5' to 3' region of CFS-FRA16D showing aberrant probe patterns in individual DNA molecules.

Figure 1

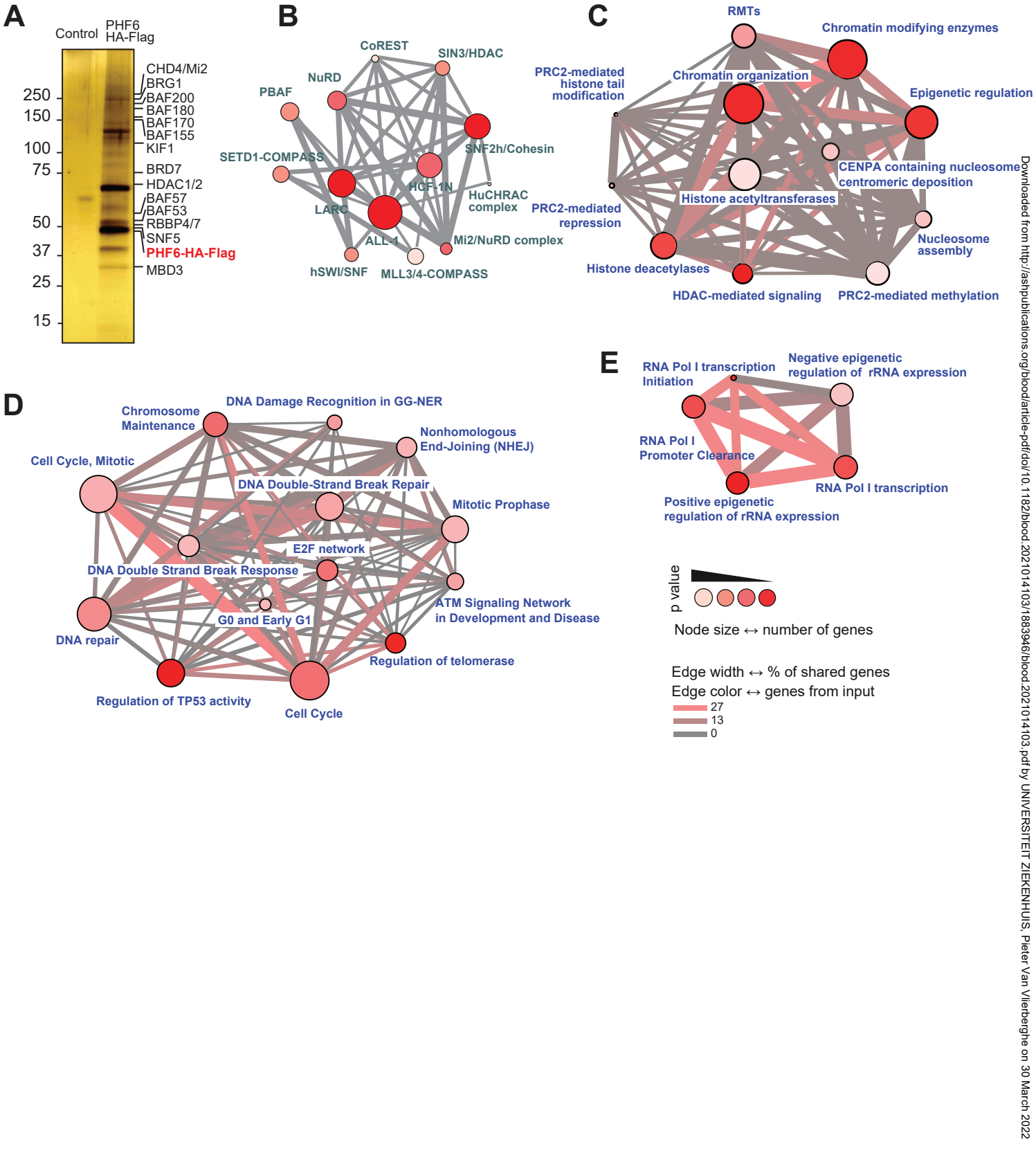

Figure 2

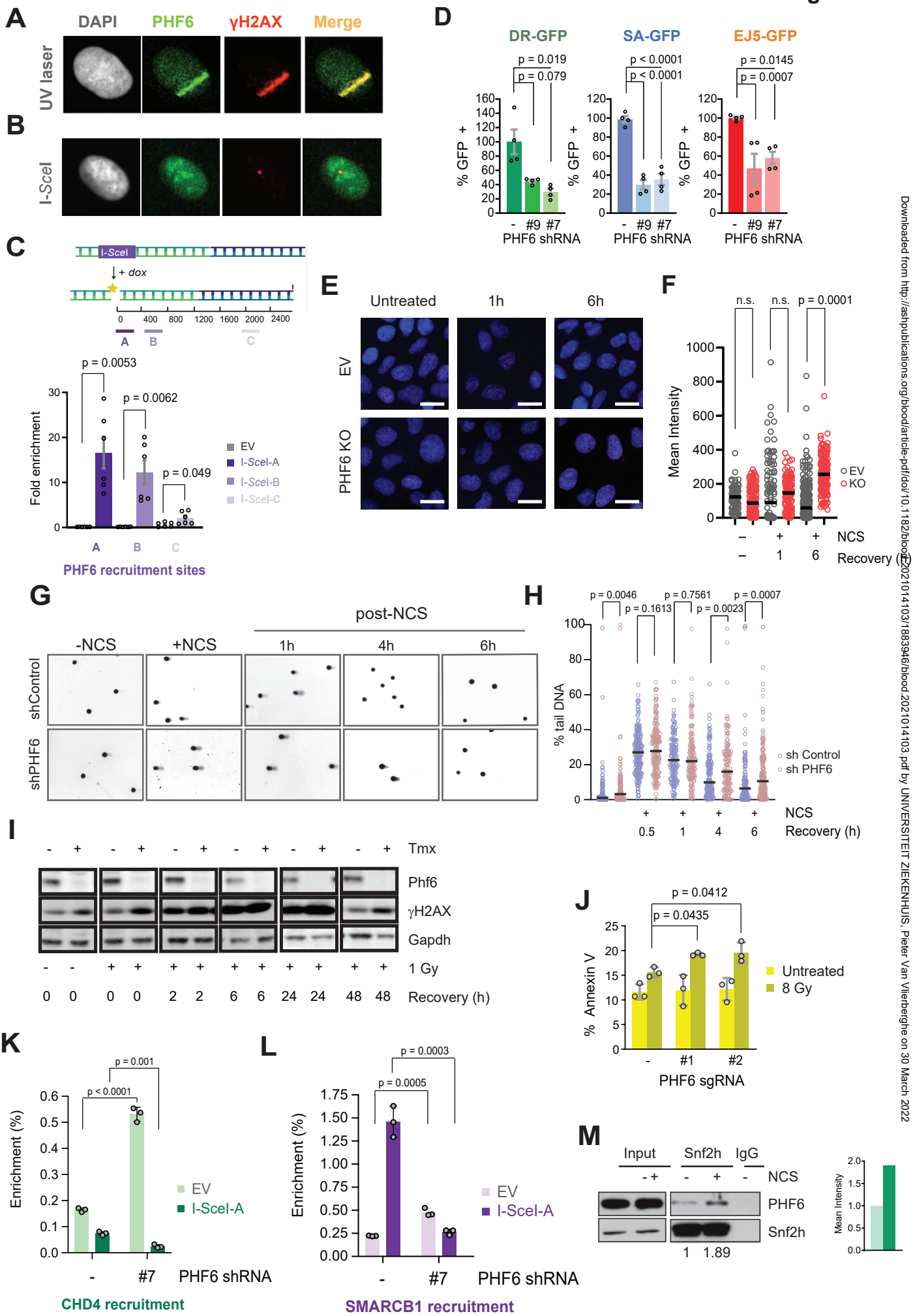

Figure 3

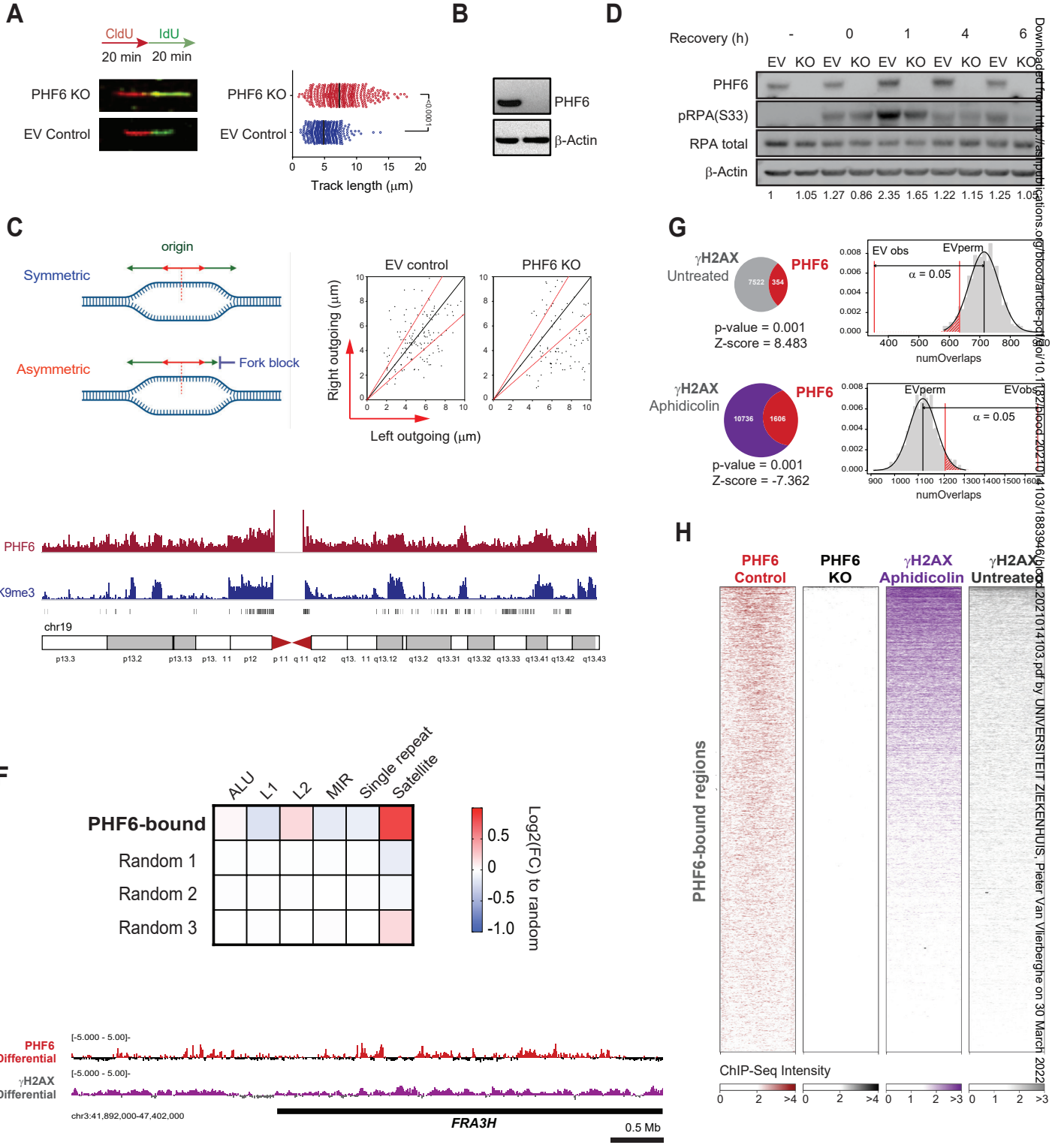

Figure 4